Chapter 6. Solvated Gas Phase Ions

6.1. Introduction

Solvated gas phase ions can serve as model systems that bridge the gap between gas phase and solution phase. In this chapter, several studies of such model systems are presented. As the scientific rationale behind each study is different, the introductions for each section will be presented sequentially.

Differential Solvation of Isomers

Section 6.3.1 deals with differential solvation of isomers, both constitutional isomers and diastereomers. Typically mass spectrometry provides mass-to-charge information about a compound, which enables assignation of an empirical formula but does not provide information about the types of functional groups present in a molecule. However, the knowledge of a compound's structure and chirality is of vital importance to the chemist. Previous work has often focused on the desire to differentiate between chiral isomers. Often, chiral host molecules are complexed with an analyte in solution or in the gas phase. This complex will then have different properties depending on the chirality of the analyte, and can be analyzed through ionization efficiencies,[1] dissociation rates,[2] or displacement rates of the analyte by a third molecule.[3,4] Isomers (although not enantiomers) can also be distinguished, in some cases, by using resonance-enhanced multiphoton ionization (REMPI) and examining the metastable ions that result from this excitation.[5] Another method of distinguishing isomers through their solvated mass spectra is presented. One advantage this method holds over previous work is that a specific functional group (that of a primary amine) can be quickly and easily identified, with very little prior knowledge of the structure of the compound.

In addition to the desirability of quickly and easily distinguishing isomers, the study of solvated isomers can potentially provide information about how chiral information might be disseminated through solution. The organization of solvent molecules around a solute molecule has been postulated to play a role in diffusion controlled reactions, taste persistence, and the action of antifreeze agents.[6] Fidler *et al.* examined several chiral camphor derivatives using both molecular dynamics and circular dichroism studies.[7] They found that these molecules could induce temperature-dependent chiral organization in achiral solvents such as CCl_4 and $CHCl_3$. Theoretical studies of water structuring by chiral solutes have also been performed using cellular automata.[6,8] Chiral molecules are simulated as square cells whose sides each have different rules governing the probability of movement of water molecules toward the cell and the probability of water molecules breaking away from the cell. The effect of the chiral cell on surrounding water extended to corner cells, but did not significantly change the occupancy by water molecules of more remote sites.[6] A second cellular automata study created an asymmetric pattern of side chains in a square arrangement (differing in the rules governing their water interactions, as above) and determined that enantiomeric species were held with differing degrees of strength, depending on their chirality.

In Section 6.3.1, a solvated primary amine (*n*-octylamine) is compared to a solvated secondary amine (dibutylamine), and the marked differences in their distribution of water molecules can be used to discriminate between the two isomers. In addition, the diastereomeric pair L-leucyl-D-tyrosine and D-leucyl-D-tyrosine are studied and their solvation patterns are compared. These very similar biological molecules show distinct differences in their solvation patterns that might demonstrate their ability to locally organize solvent molecules.

Solvated Alkylammonium Ions

In Section 6.3.2, studies of solvated quaternary alkylammonium ions are presented. These species were chosen for this study because of their importance as structure-directing agents in zeolite formation, a process that is incompletely understood.[9] Symmetric tetraalkylammonium ions are often used to direct zeolite crystal growth. Very slight changes in the structure of the organic species can result in dramatic changes in the final crystal structure. Figure 6.1 shows how the zeolites resulting from the use of tetraethylammonium (TEA) differ dramatically from those resulting from the use of tetrabutlyammonium (TBA). The sensitivity of the crystal structure to small changes in the organic templating reagent is used by researchers to determine how new zeolite structures can be produced.

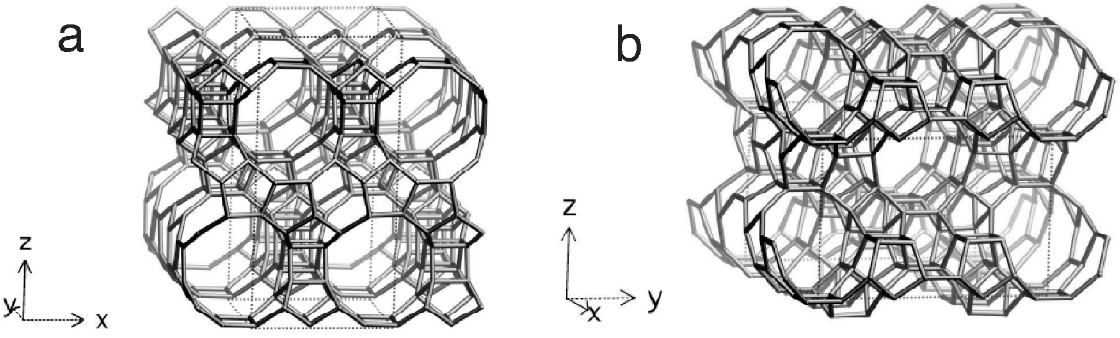

Figure 6.1. (a) The zeolite BEA, produced from TEA. (b) The zeolite ZSM-11 (MEL structure), produced when TBA is used as a structure-directing agent. Zeolite structures from www.iza-structure.org/databases.

Alkylammonium cations in aqueous solutions are believed to order the water molecules around them in a process referred to as hydrophobic hydration. In this process, the hydrophobic nature of the alkyl chains causes the probability of hydrogen bonding of waters in the vicinity to increase. This might favor the formation of stable water cages, or clathrate hydrates, around the alkylammonium ion solutes.[10] Raman studies suggest that at room temperature, hydrophobic hydration plays a limited role, but as the temperature is decreased clathrate-like structuring around R_4N^+ ions becomes increasingly apparent.[11] A sequence of solvated symmetric tetraalkylammonium ions is examined in Section 6.3.2 and the existence of possible clathrate-like structures is discussed.

In addition, two doubly charged quaternary ammonium ions are also examined. The first few enthalpies of hydration of doubly charged diamines and alkylammonium ions have been examined by Kebarle *et al.*[12] They observe that the charged sites in the doubly protonated diamines are sequentially hydrated, such that the first two water molecules attached to the ion have essentially equal heats of hydration, as do the second two water molecules. The authors observe that this equality holds for $H_3N(CH_2)_pNH_3^{2+}$ while $p > 6$. The molecules $(CH_3)_3N(CH_2)_pN(CH_3)_3^{2+}$, where $p = 2 - 6$, were also examined, although hydration enthalpies could not be obtained for $p > 3$, and the data are less accurate than those obtained for the diamines. It remains unclear whether the tetraalkylammonium dications also hydrate sequentially by charge site, or whether the lack of hydrogen binding sites in the tetraalkylammonium species causes waters to bind to each other after the first water molecule has been attached to the ion. Meot-Ner and Deakyne conducted theoretical studies on alkylammonium ions indicating that the second water associating with tetramethylammonium ion will interact preferentially with the first water molecule, rather than binding to the tetramethylammonium ion,[13] but these simulations were not conducted on doubly charged species and may be of limited relevance. Results of photoelectron spectroscopy studies on a doubly charged anion, $^{-}O_2C(CH_2)_6CO_2^{-}$, indicate that this molecule solvates each charge site alternately.[14,15] When 16 water molecules are associated with the dianion, the conformation of the molecule changes from an open conformation to a folded conformation, as the attraction between water molecules overcomes the intramolecular Coulomb repulsion and pulls the negatively charged carboxylate groups closer together.

Solvolysis of *t*-Butyl Chloride in Water Clusters

Finally, in Section 6.3.3, uptake of *t*-butyl chloride by protonated water clusters and the subsequent reaction of *t*-butyl chloride with water to lose HCl from the water cluster are examined. Water clusters are an intermediate phase between the gas phase, where stable ions have delocalized charge, and solution, in which stable ions are typically compact and highly solvated. They are thus useful model systems for understanding how water interacts with ions, and how many water molecules are needed to effect the transition from gas phase behavior to solution phase behavior.

A recent review on this topic by Bondybey and Beyer[16] highlights the work done on reactions within water clusters. These reactions include, for example, ionic dissociation of acids,[17] redox reactions,[18-21] precipitations,[22] and base catalyzed aldol reactions.[23] Typically in such experiments, water clusters are formed using a supersonic expansion technique. Metal cations can be introduced via laser ablation of a metal source, and neutral molecules can be introduced into the experimental apparatus (typically an ion trap). This method of introducing reactants to a water cluster works well for hydrogen bonding species, which can exchange with some of the water ligands in the cluster, but fails for highly volatile molecules. In order to avoid these obstacles, and to introduce neutral reactants into water clusters before the clusters are cooled, we use an electrospray source to produce protonated water clusters and expose the electrospray plume to a vapor of the neutral reactant (in this case, *t*-butyl chloride).

S_N2 reactions are fundamental reactions in organic chemistry, and have been studied in both solution and the gas phase. The presence of solvent has a strong effect on these types of nucleophilic substitution reactions, as polar solvent molecules stabilize the reactants and products in comparison to the transition state. This generally has the effect of slowing the reaction in solution relative to the gas phase. The difference in rate constant between solution and gas phase S_N2 reactions can be as much as 20 orders of magnitude.[24,25] Bohme and Raskit have examined the reaction of $OD^-(D_2O)_n$ with CH_3Cl in a flowing plasma mass spectrometer, where n ranged from 0 to 3, and found that the rate of reaction decreased by at least three orders of magnitude (beyond the measuring capabilities of the spectrometer) when the anion was solvated by only two or three waters.[26] Theoretical studies on this reaction were also conducted for $n = 0$, 1, and 2 water molecules, and the transition state for methyl inversion for $n = 2$ was found to have an energy comparable to the energy of reactants, while the $n = 0$ and $n = 1$ species had transition states lower in energy than the reactants.[27] There is general consensus that transition structures are less strongly solvated than reactants when waters are explicitly included in a reaction.[28,29]

S_N1 reactions have been difficult to study in the gas phase, due to the fact that they demand dissociation of one of the reactants before the (fast) reaction step. The solvolysis of *t*-butyl chloride has been examined computationally.[30-32] Jorgensen and coworkers found that the contact ion pair of *t*-butyl cation and chloride anion is separated at a distance of 2.9 Å and that water molecules can be inserted between the ions when they are separated at a distance of 5.0 – 5.5 Å.[30] Okuno found that for a cluster of four water molecules and *t*-butyl chloride, the water molecules form a "relay network" in which the back side of the central carbon of the *t*-butyl group is nucleophilically solvated and the remaining waters are hydrogen-bound to the water solvating the *t*-butyl carbon such that the last water in the chain electrophilically solvates the chloride anion.[32] Yamabe and Tsuchida determined that the most effective relay network was made up of four water molecules.[31] They also find that intermediate C-OH distances are unstable, and that solvation of the *t*-butyl chloride by nucleophilic water, enhanced by a hydrogen bond network, results in formation of a covalent C-O bond; that is, the *t*-butyl cation is not a stable intermediate when solvated by a water molecule. The chloride ion is then displaced away from the *t*-butyl center and HCl is formed.

6.2. Experimental

All experiments were performed in an external ion source 7T FT-ICR mass spectrometer that has been described in detail elsewhere.[33] Briefly, the instrument is equipped with a RF-only octopole ion guide, which transfers the ions from the atmospheric pressure ion source into the ICR cell. An electromechanical shutter that is located between the ESI source and the octopole was opened for two seconds to allow ions continuously being generated by the ESI source to enter the octopole ion guide. The RF field of the octopole was turned on only during this period of time. Argon collision gas (2 – 5 ms pulse, 10^{-6} torr) was introduced to moderate the ion kinetic energy while the ions were traveling through the octopole ion guide and subsequently trapped in the ICR cell. For production of hydrated ions a modified version of a commercially available electrospray ion source (Analytica of Branford, Branford, CT) was used that has been described elsewhere.[34] Species of interest were dissolved in pure deionized water containing 0.01% acetic acid at concentrations around 100 μM. A syringe pump (Harvard Apparatus, Model PHD 2000, South Natick, MA) injects electrospray solution through a hypodermic stainless steel capillary (63 μm i.d.) at a flow rate of 80 – 150 nl/min. A potential of 1000 – 2000 V at the entrance cap of the desolvation capillary with respect to the grounded needle initiates the spray. The onset voltage depends on the polarity of the sample solution. The distance between the spray needle and the desolvating capillary is about 2 mm and can be adjusted by the experimenter to optimize the spray during experiments. No nebulizer or counterflowing drying gas was used and the desolvation capillary is operated at room temperature. Chemicals were purchased from Aldrich Chemical Company (Milwaukee, WI) and used without further purification, except for the compounds SDA 114, CBD-6, and SDA 162, which were obtained from the Mark Davis lab at Caltech. To examine the behavior of *t*-butyl chloride in water clusters, the *t*-butyl chloride was placed in a shallow container beneath the electrospray apparatus and its vapor entered the electrospray plume. In this way, the neutral reactant was introduced into water clusters before evaporation occurred, and the problem of effecting ligand exchange with water was avoided.

6.3. Results and Discussion

6.3.1. Discrimination between Isomeric Species by Differential Solvation

Mass spectrometry provides no direct structural information, making it difficult to distinguish between isomeric compounds. We have been able to produce solvated ions and observe evaporation of water molecules from solvated species. For protonated water clusters, magic numbers are observed at $n = 21$, 28, 51, 53, and 55. These cluster at $n = 21$ has been assigned as a clathrate in which 20 waters form a pentagonal dodecahedron encapsulating a hydronium ion (**6.1**).[34-36] The cluster at $n = 28$ has been attributed to a pentakaidecahedron with a proton-bound water dimer contained within the cluster (**6.2**). The larger clusters might be ice-like structures, or may be more complex clathrates with face-sharing polyhedra, capable of enclosing various numbers of neutral and/or ionic species in cavity voids. For example, **6.3** is a neutral clathrate consisting of 51 water molecules, which might enclathrate a proton-bound dimer that would account for the magic number at $n = 53$. Ammonia clusters $NH_4^+(H_2O)_n$ show magic numbers at $n = 20$, 27, 50, 52, and 54, suggesting that the ammonium ion can be enclathrated much as a hydronium ion is in pure water clusters.[34,36] These magic numbers are also found in spectra of solvated primary amines, indicating that a protonated amine group replaces one of the waters in a clathrate structure.

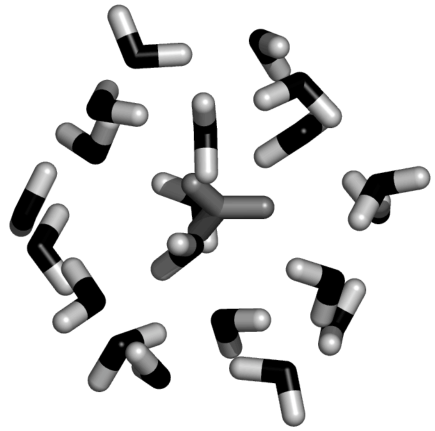

6.1

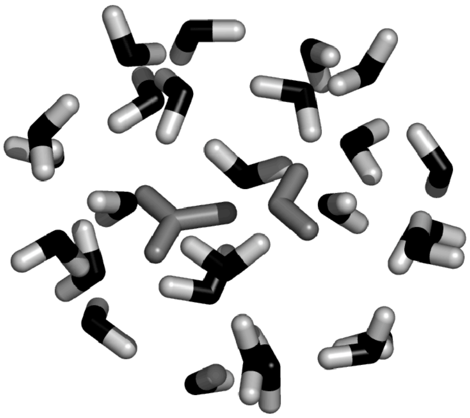

6.2

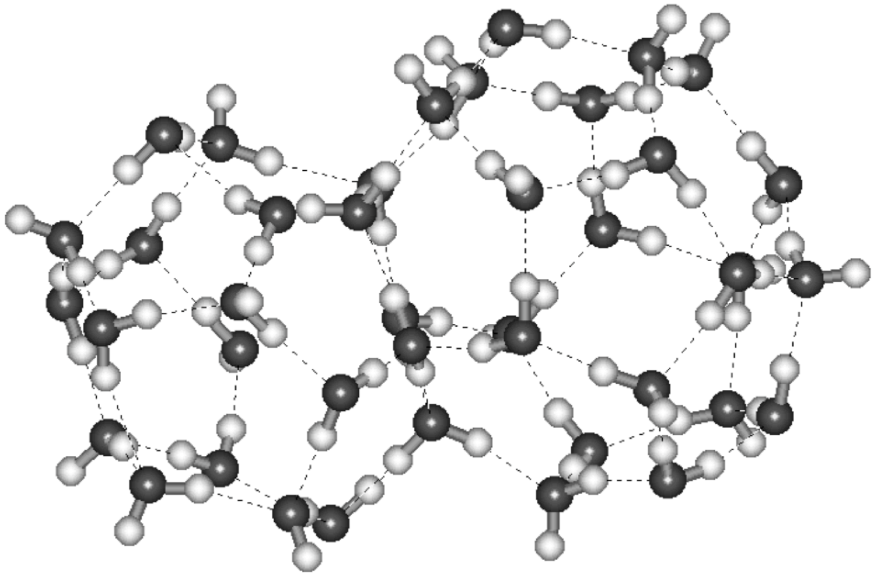

6.3

The magic numbers present in the mass spectra can be used to discriminate between constitutional isomers. Figure 6.2a shows a mass spectrum of solvated *n*-octylamine, and Figure 6.2b is the mass spectrum obtained of solvated di-*n*-butylamine. The spectrum of *n*-octylamine exhibits "magic numbers" corresponding to unusually stable ion-water molecules clusters at n = 20, 27, 50, 52, and 54, as is expected of a primary amine. In contrast, the secondary amine spectrum shown in Figure 6.2b does not show magic numbers until *n* is large (*n* = 47, 51, 53). The additional steric hindrance found in the secondary amine probably precludes it from taking the place of a water molecule in the clathrate structure, explaining the lack of magic numbers in the low *n* portion of the spectrum. In this case, a brief examination of the mass spectra of two constitutional isomers enables discrimination between a primary amine and a secondary amine.

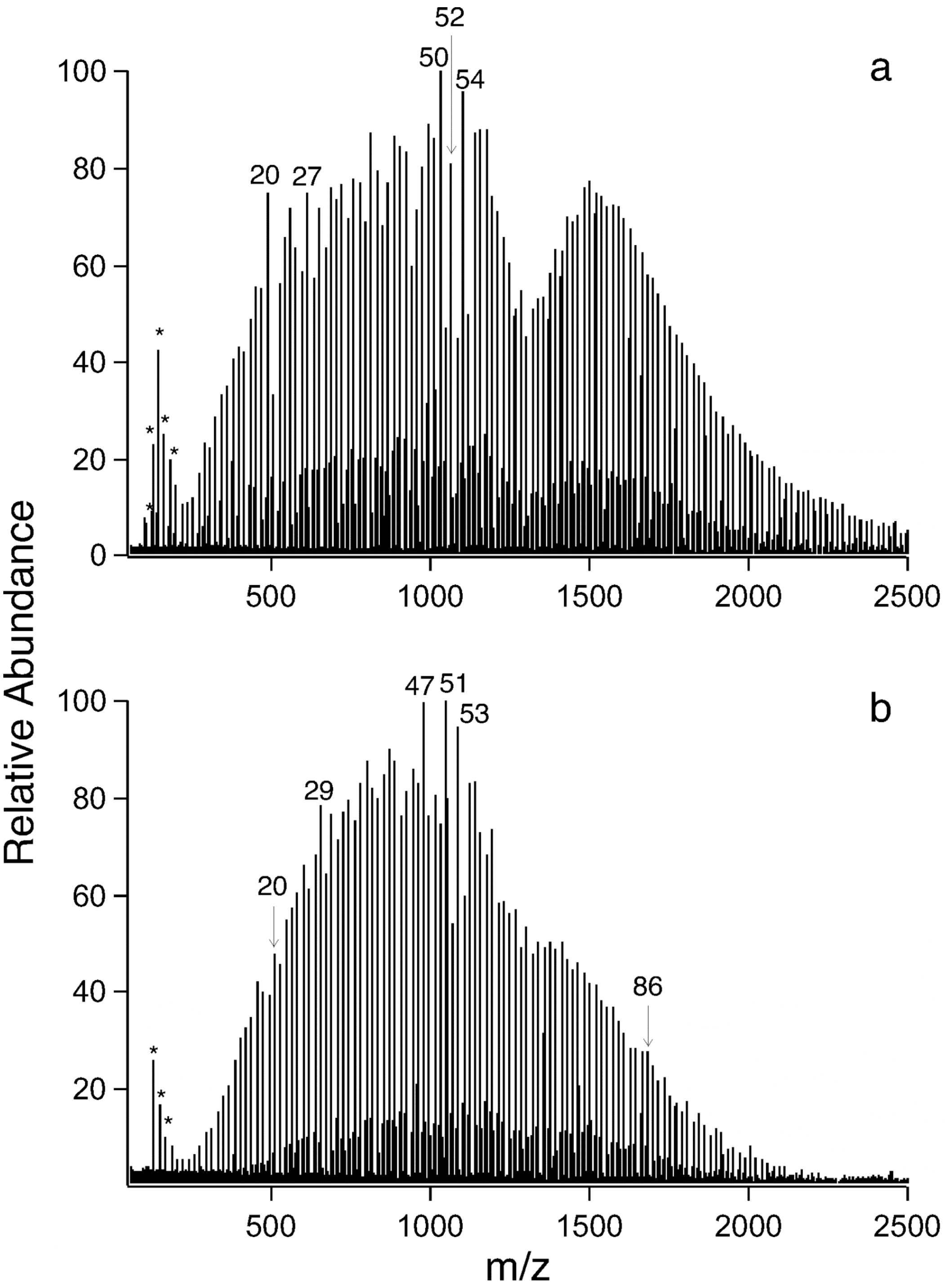

Figure 6.2. (a) Distribution of water clusters containing protonated *n*-octylamine after 8 seconds of evaporation. (b) Distribution of water clusters containing protonated dibutylamine after 8 seconds of evaporation. Asterisks indicate impurities.

The behavior of diastereomers was also examined. The species D-leucyl L-tyrosine and L-leucyl L-tyrosine are diastereomers, differing in the chirality of the leucine residue. As such, they are expected to have different physical properties, In this case, there are few magic numbers indicating unusually stable clusters in the mass spectrum, as shown in Figure 6.3. To compare fine details in the pattern of solvated molecules, it is useful to plot the intensity ratio $[M(H_2O)_n^+]/[M(H_2O)_{n+1}^+]$ as a function of the number of waters (n) to determine which species are relatively stable. Evaporation of water molecules from the observed species is occurring inside the ICR cell in a stepwise fashion;[34] if one configuration, $M(H_2O)_x$, is more stable than others, there will be a tendency for the evaporation of the $M(H_2O)_{x+1}$ cluster to proceed more readily than otherwise. This is reflected in a relatively larger intensity ratio. The ratios of the intensities of the water clusters for D-leucyl-L-tyrosine and L-leucyl-L-tyrosine after 20 seconds of evaporation are shown in Figure 6.4. No "magic number" clusters with intensity ratios greater than 1.5, such as those seen in the spectra of *n*-octylamine in Figure 6.2a for 20, 50, and 52 waters around a central ion, are observed in the spectra of leucyl tyrosine. However, there are small but pronounced and reproducible differences between the diasteromeric species. For example, the intensity ratio $[M(H_2O)_{25}^+]/[M(H_2O)_{26}^+]$ is significantly larger for D-leucyl-L-tyrosine than for L-leucyl-L-tyrosine after 20 seconds of evaporation. (Error bars are larger for large numbers of water molecules because the signal intensity diminishes for very large water clusters.)

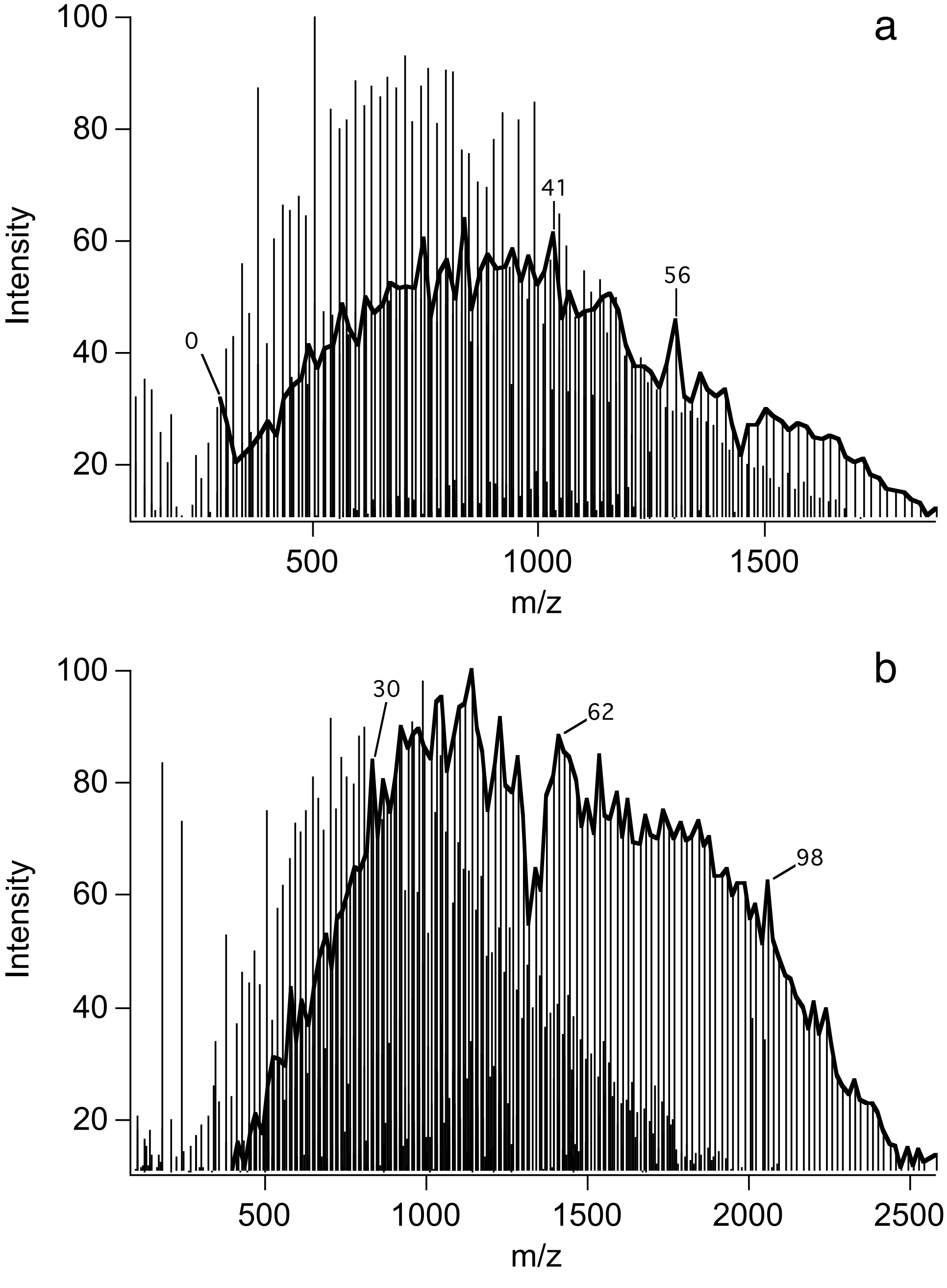

Figure 6.3. (a) Mass spectrum of D-leucyl-L-tyrosine after a 20 second delay. (b) Mass spectrum of L-leucyl-L-tyrosine after a 20 second delay. The black lines guide the eye to the solvated dipeptides. Numbers refer to the number of water molecules associated with the dipeptide.

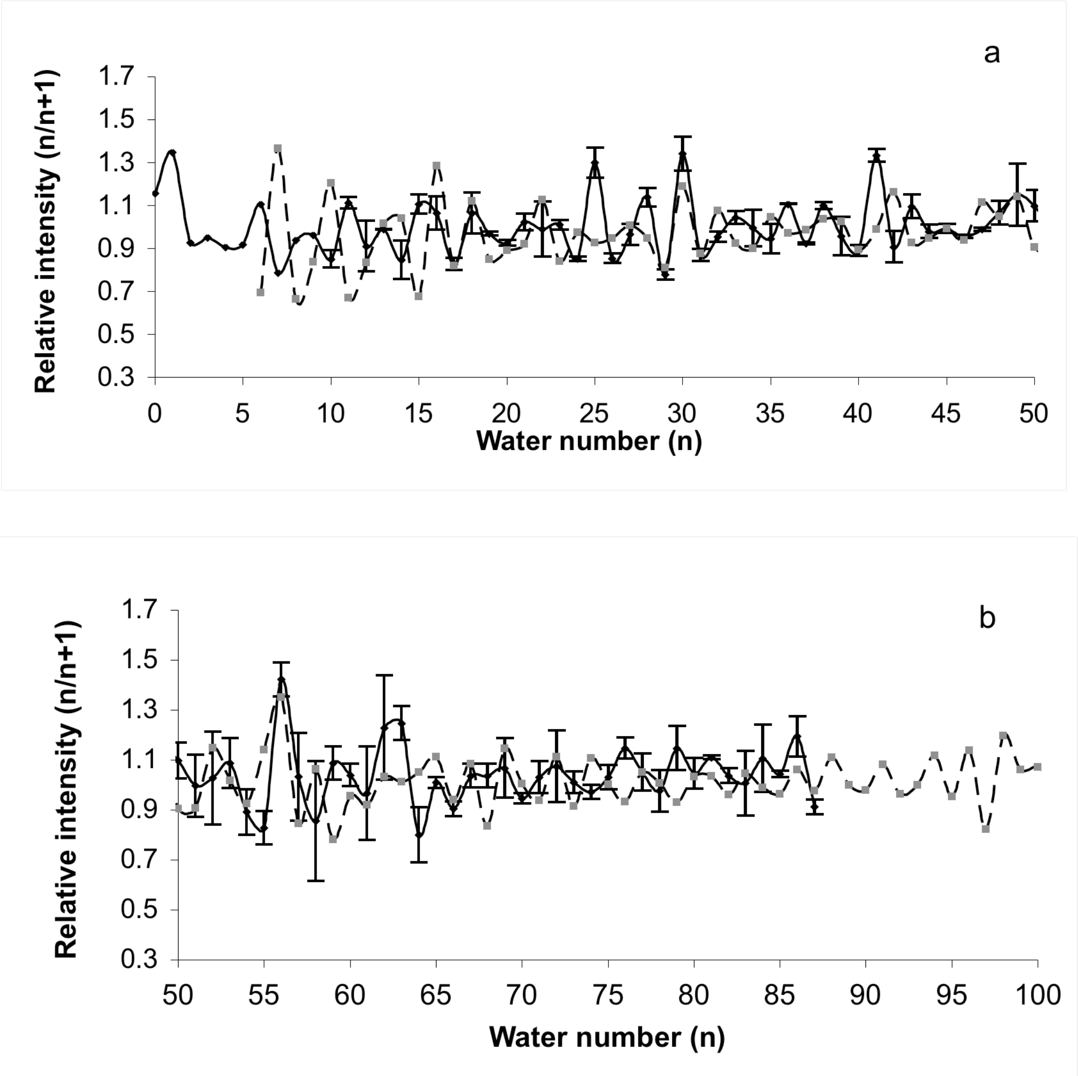

Figure 6.4. (a) Relative intensity of water clusters (*n* = 0 – 50) after 20 s delay. L-leucyl-L-tyrosine data are shown in gray, while D-leucyl-L-tyrosine data are shown in black. Error bars from repeated trials are included for the DL data. (b) Relative intensity of water clusters (*n* = 50 – 100) after 20 s delay.

These trends persist as water molecules evaporate from the cluster. Figure 6.5 shows the relative intensities of water clusters after 25 seconds of evaporation. Again, the relative intensity of the *n* = 25 cluster is larger for the D-leucyl-L-tyrosine species than for L-leucyl-L-tyrosine. This feature is also present in the data 30 seconds after evaporation (data not shown). The same is true for the *n* = 30 cluster. Other features persist until 40 seconds after evaporation; for example, the relative intensities of the *n* = 1, 2, and 3 water clusters are consistently larger for the D-L species than for the L-L species until 40 seconds after evaporation, after which these water clusters evaporate. These differences in stabilities may indicate that the diastereomers are patterning the water around them differently; for example, the D-L species might be able to bind certain numbers of water molecules more effectively than the L-L species. In either case, the chiral molecules are showing distinct and reproducible differences in their solvated mass spectra that suggest they are able to locally organize solvent molecules.

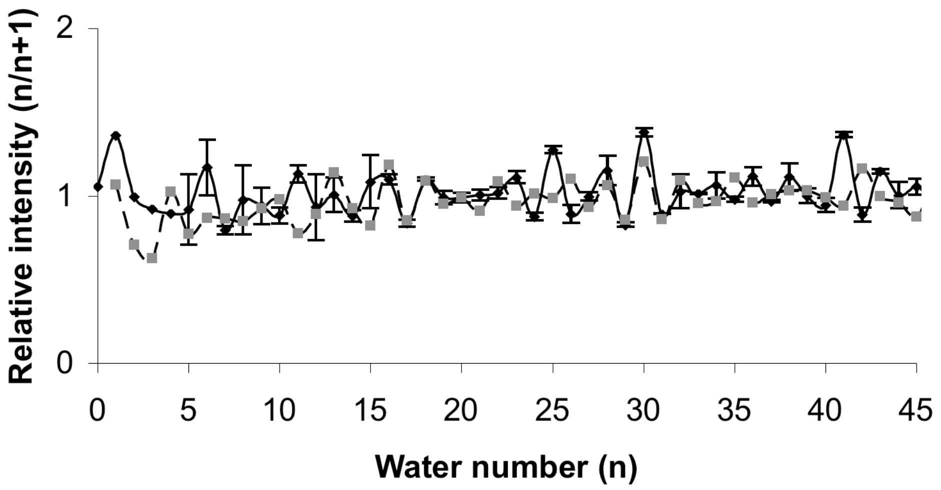

Figure 6.5. Relative intensity of water clusters (*n* = 0 - 45) after 25 s delay. L-leucyl-L-tyrosine data are shown in gray, while D-leucyl-L-tyrosine data are shown in black. Error bars from repeated trials are included for the D-L data.

6.3.2. Water Clusters of Alkylammonium Structure-Directing Agents

Bromide salts of a series of tetralkylammonium ions (TAA; $N(C_nH_{2n+1})_4^+$, $n = 1$ to 8) were studied to determine the presence of any particularly stable hydrated species. The hydration behavior of several more complex structure-directing agents was also studied. Some typical spectra obtained using the super-soft ESI source with the FT-ICR are shown in Figure 6.6 for tetraethylammonium (TEA). The tallest peaks in the spectra are due to $TEA^+(H_2O)_n$ species; the fine structure is due to $H^+(H_2O)_n$ and $NH_4^+(H_2O)_n$ species. As the hydrophobicity of the solvated species increases, the solvated proton and ammonium clusters dominate more of the spectrum. When $n > 80$, the distribution smooths and fewer magic numbers are observed. This may be due to the shielding effect of waters closest to the ion being solvated, reducing the apparent charge to waters outside of this first solvation layer.

It is also interesting to note that TEA shows a marked magic number at $n = 28$. Self-diffusion measurements have shown that in aqueous solution TEA coordinates about 30 water molecules.[38] The species observed in the gas phase might reflect the coordination of water molecules to the alkylammonium ion solute that occurs naturally in solution.

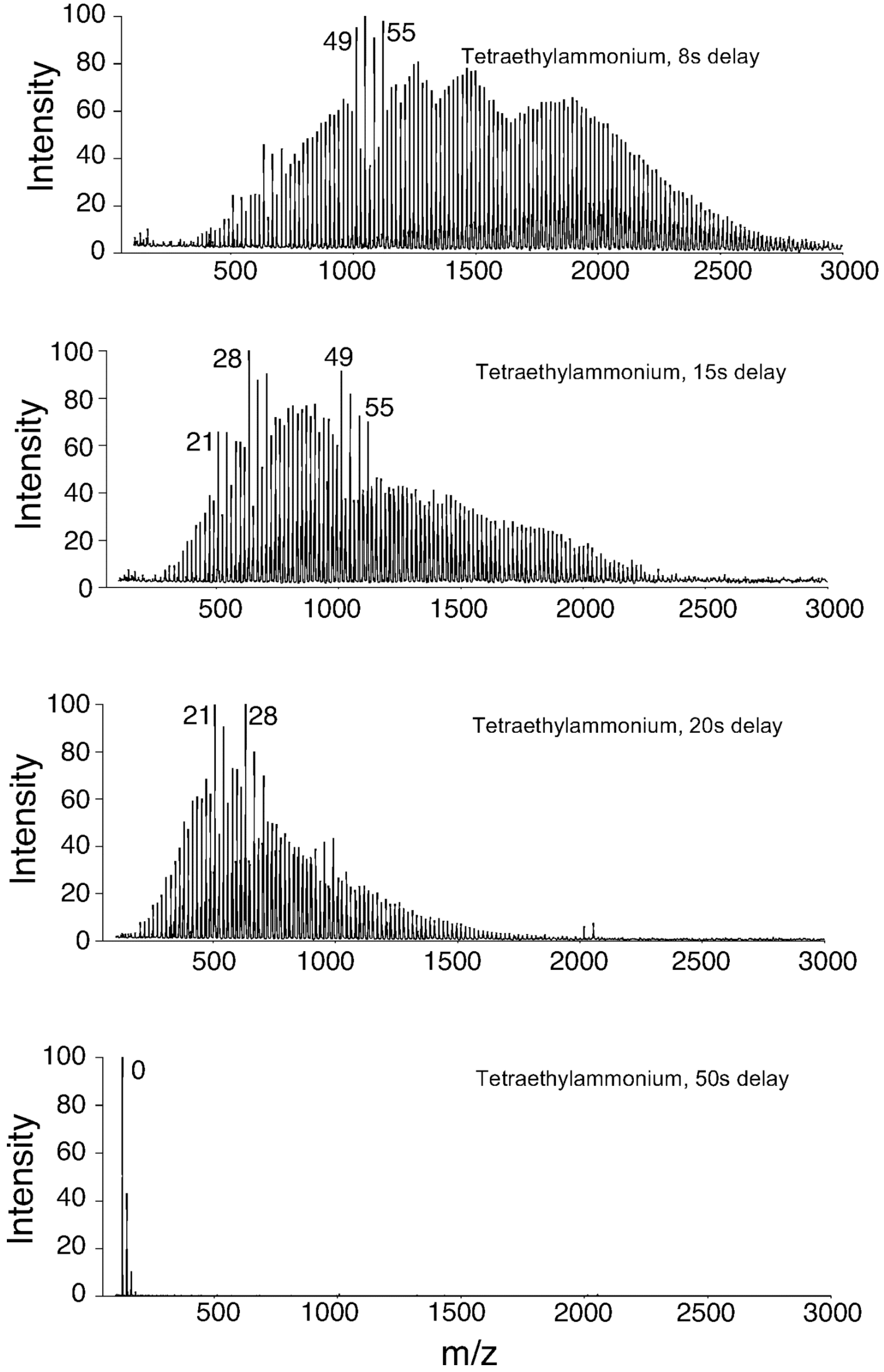

Figure 6.6. Signal intensity as a function of mass-to-charge ratio for solvated TEA at various delay times between capture and detection. Marked peaks correspond to TEA$^+$(H_2O)$_n$, where *n* is labeled on the figure.

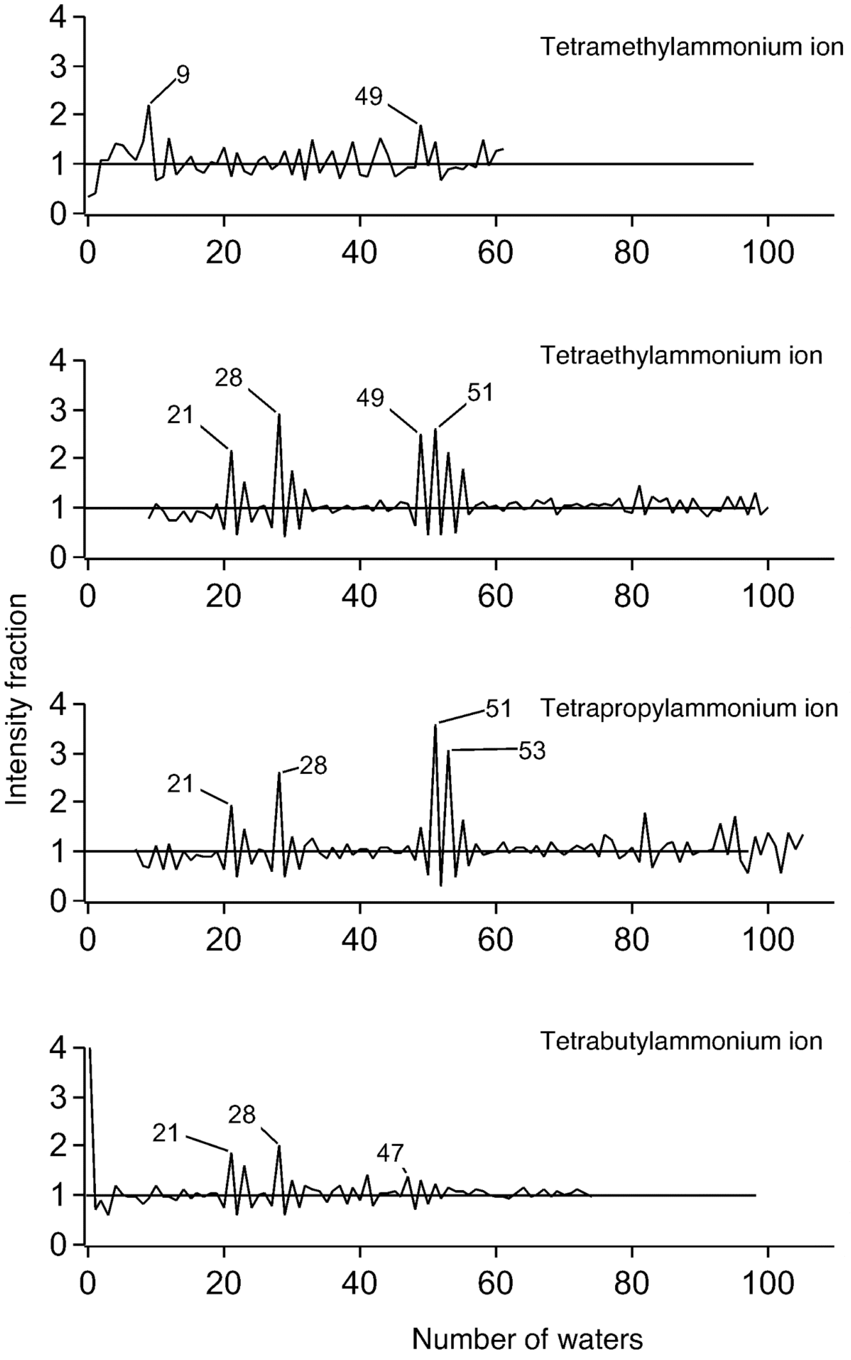

Figure 6.7. Intensity fraction $[M(H_2O)_n^+]/[M(H_2O)_{n+1}^+]$ as a function of n for TAA cations. All data are taken with a 15 second delay between capture and detection. Note the characteristic "magic numbers" at 21, 28, 51, and 53 for TEA and TPA, and those at 21 and 28 for TBA.

Data were collected on the series of cations $N(C_nH_{2n+1})_4$ for $n = 1, 2, 3, 4, 5, 7$, and 8. To compare the results for these TAAs, the intensity fraction is plotted as in Section 6.3.1. Figure 6.7 shows intensity ratio plots for tetramethyl ammonium (TMA), TEA, TPA, and TBA. Excepting TMA, there are prominent magic numbers (stable peaks) for where 21, 28, 51, and 53 water molecules are associated with the alkylammonium species, although TBA does not exhibit strong magic numbers for $n = 51$ and 53. The most prominent magic numbers occur in the case of TPA. Figure 6.8 shows the intensity ratio plots for tetrapentylammonium ion (TPenA), tetraheptylammonium ion (THepA) and tetraoctylammonium ion (TOA). Tetraheptylammonium ion shows almost no indication of having magic numbers in its spectrum, and the magic numbers at $n = 21$ and 28 are lower in the TOA spectrum than in those of the smaller alkylammonium ions. This may correspond to an increase in hydrophobicity as the chain length increases. The average number of water molecules at 15 seconds after capture does not correlate well with chain length as a measure of hydrophobicity, most likely because the initial cluster distributions are extremely sensitive to instrumental parameters and external factors such as relative humidity. The results for TMA may be explained by considering the degree of charge screening by the alkylammonium ions. The methyl groups attached to the nitrogen center should not provide the same level of charge screening as the larger alkyl groups. This may expedite water bonding to the quaternary ammonium ion and prevent water molecules from assembling into a stable clathrate framework that can associate with the ion.

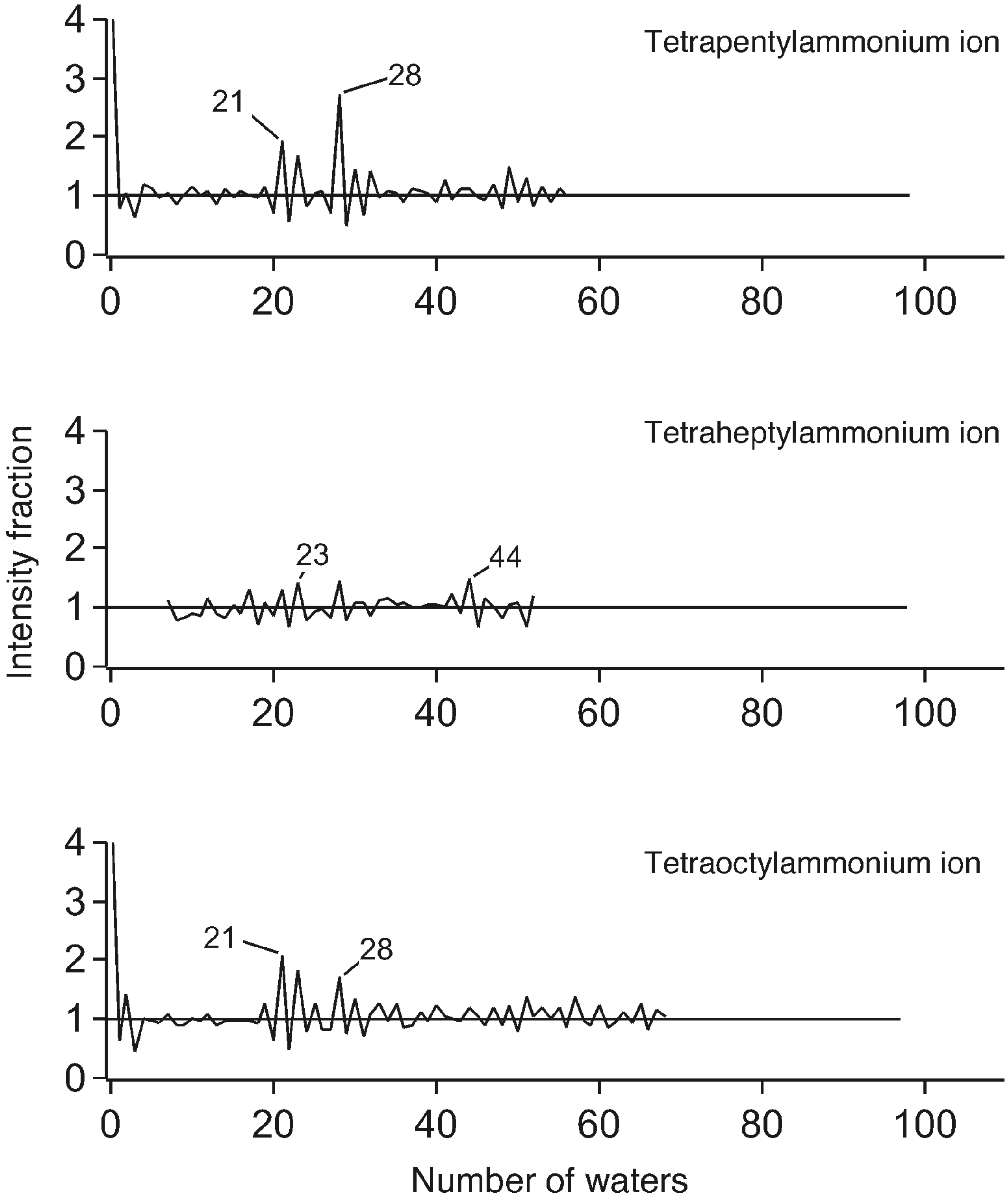

Figure 6.8. Intensity fraction $[M(H_2O)_n^+]/[M(H_2O)_{n+1}^+]$ as a function of n for tetrapentylammonium, tetraheptylammonium, and tetraoctylammonium cations. All data are taken with a 15 second delay between capture and detection.

Lee *et al.*[34] have suggested that the prominent magic numbers at 21 and 28 are due to ion-cluster interactions between an ion and a relatively stable neutral water clathrate (Figure 6.9). For $n = 21$, a pentagonal dodecahedron with a neutral water molecule encapsulated within could be complexed with the ion; for $n = 28$, a 28-mer water cluster, or a 26-mer water cluster with a neutral dimer encapsulated, could complex with the ion.

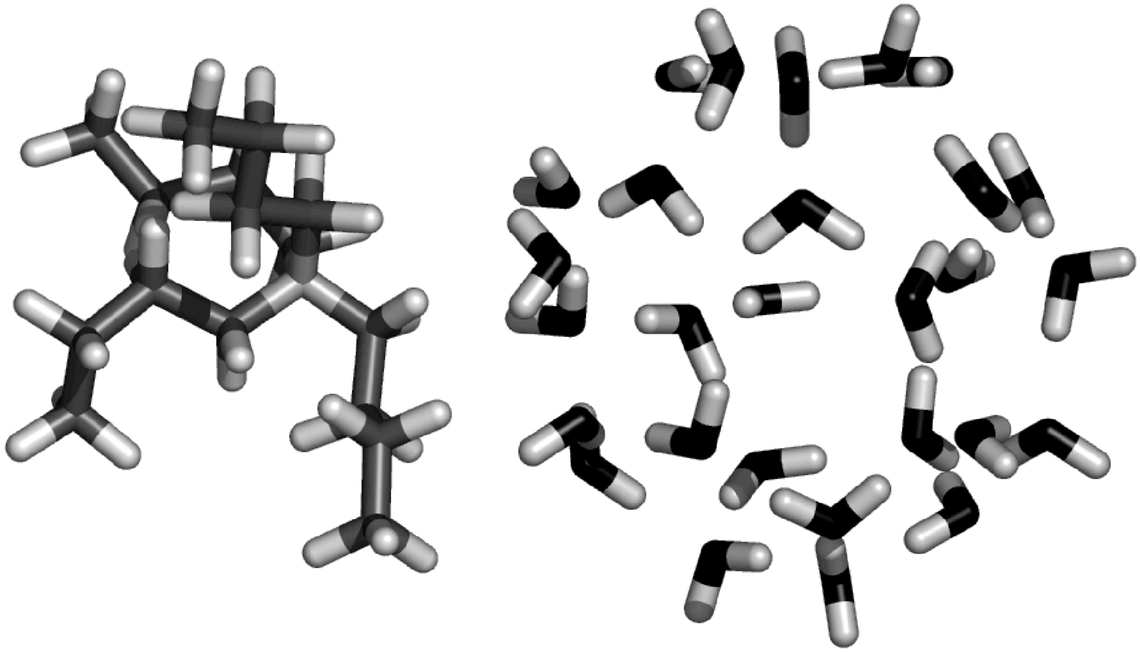

Figure 6.9. A 28-water ion-cluster complex with TBA. The 28-water species is most prominent in TEA, TPA, and TBA.

Some more complex organic ammonium compounds synthesized by Mark Davis's lab were also studied.[†] Intensity fraction plots for these species and the structures of the species are shown in Figure 6.10. SDA 114 directs the formation of an amorphous molecular sieve (no clear crystal structure is obtained). The most stable water

---

[†] Precursor solutions containing a structure-directing agent and silicic acid were also examined using ESI-MS, in an attempt to identify nascent zeolite structures. The results of these experiments were inconclusive, at best, and so are not included in this thesis.

clusters seem to occur when larger numbers of waters are associated with this species, which may account for its ability to direct (even amorphous) zeolite formation. CBD-6 (the first structure directing agent shown) directs the formation of MFI-type zeolites, such as ZSM-5. Because this molecule is a diquaternary ammonium cation, we expect that as waters evaporate, increased Coulombic repulsion between the two charge centers would cause the molecular species to extend and stable structures formed by ion-water interactions would consequently be destroyed. There is a distinctly oscillatory quality to the relative intensity data from $n = 38$ onward, where species with even numbers of water molecules are consistently more stable than those with odd numbers of water molecules. This may imply the waters cluster around both cationic sites and are lost from each site more or less independently. This alternate solvation has been observed with fewer numbers of solvent molecules for doubly deprotonated dianions and diprotonated alkydiammonium anions.[12,15] The odd-even effect became "smeared out" in photoelectron spectra of $^{-}O_2C(CH_2)_6CO_2^{-}(H_2O)_n$ clusters where $n = 10 - 20$, but the stability results found here indicate that such a difference (albeit small) may still exist for these larger clusters.

In comparison, the decamethonium spectrum does not display an immediately recognizable structure (although, again, the even-numbered clusters are slightly more stable than the odd-numbered clusters). The spectrum of TMA does not have prominent magic numbers, and this might explain the absence of significant magic numbers in the decamethonium spectrum.

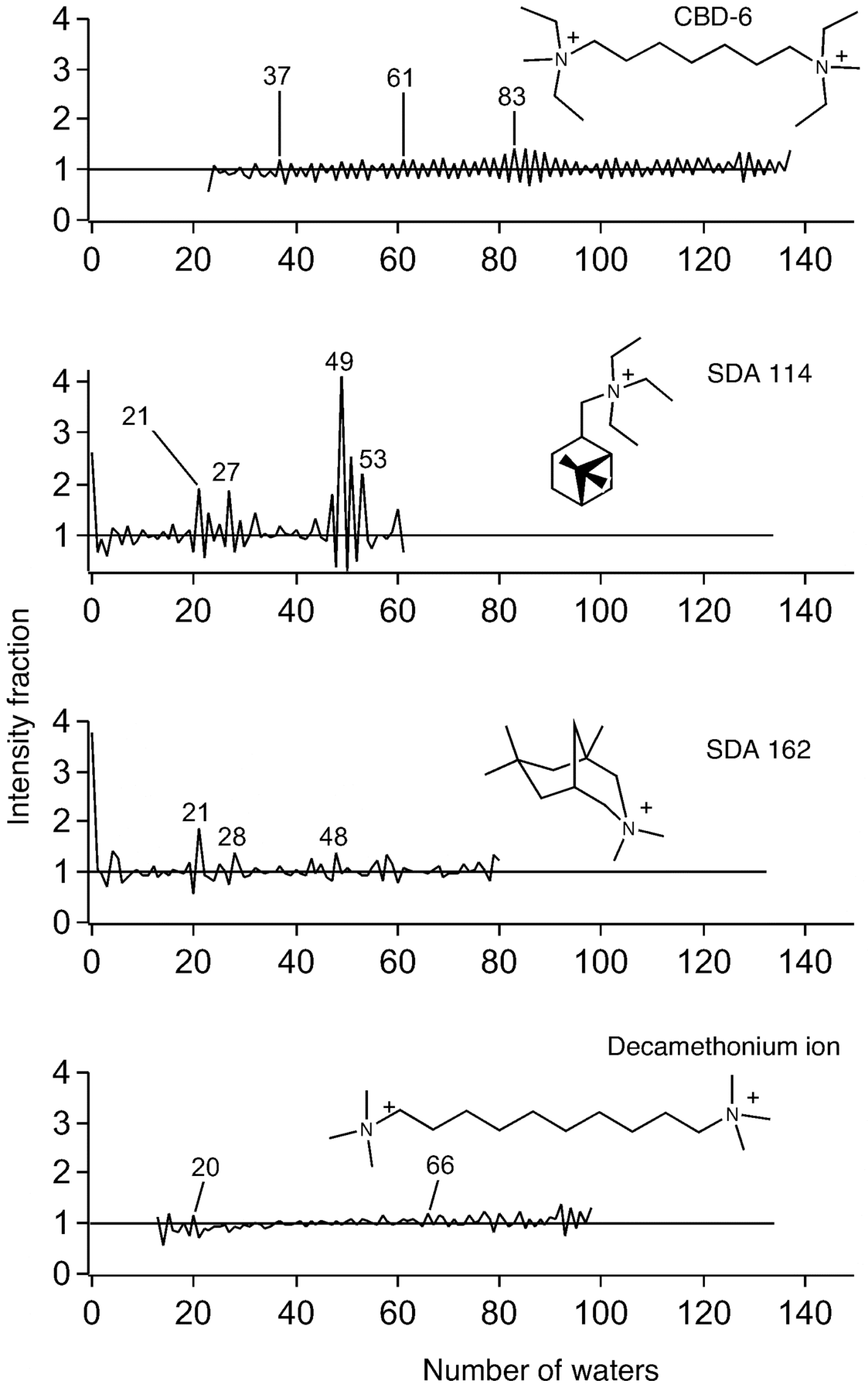

Figure 6.10. $[M(H_2O)_n^+]/[M(H_2O)_{n+1}^+]$ **as a function of** n **for various complex structure-directing agents. All data are taken with a 15 second delay between capture and detection. CBD-6 and decamethonium ions are doubly charged species.**

6.3.3. Uptake of *t*-Butyl Cation and Subsequent Reaction in Water Droplets

The *tert*-butyl species is introduced into a droplet by introducing a vapor of *t*-butyl chloride into the electrospray plume, as detailed in Section 6.2. Figure 6.11 shows the water cluster distribution obtained from such an experiment. The dominant peaks in the spectrum are due to $(H_2O)_nNH_4^+$ clusters. Clusters corresponding in mass to *t*-butyl chloride clusters can also be seen. One possible reaction expressing the uptake of *t*-butyl chloride by the electrospray plume is

$(H_2O)_nH^+ + C_4H_9Cl \rightarrow (H_2O)_nC_4H_9ClH^+$ (n very large)

As the water droplets that have incorporated *t*-butyl chloride evaporate, charged clusters are formed that contain *t*-butyl chloride, as observed in the mass spectrum shown in Figure 6.11. The *t*-butyl chloride is probably dissolved in the cluster at this point, such that the *t*-butyl cation is present and the chloride anion can associate with *t*-butyl cation and/or a hydronium ion. These clusters can further evaporate by losing water molecules sequentially. Alternatively, a reaction can occur within the cluster in which a chloride anion picks up a proton from a hydronium ion to from HCl, and the HCl molecule can be evaporated from the cluster:

$(H_2O)_nC_4H_9Cl\,H^+ \rightarrow (H_2O)_{n-1}C_4H_9ClH^+ + H_2O$

$(H_2O)_nC_4H_9Cl\,H^+ \rightarrow (H_2O)_{n-1}C_4H_9OHH^+ + HCl$

Distinguishing between clusters containing *t*-butyl chloride and those containing *t*-butyl hydroxide is difficult, since the nominal mass of HCl (36) is equivalent to that of $(H_2O)_2$. However, the exact mass of HCl is 35.97668, and the exact mass of $(H_2O)_2$ is 36.02114. FT-ICR's capability for high mass resolution allows us to distinguish between small differences in mass. While the instrument is not accurately tuned over the mass range covered in the spectrum, the $(H_2O)_nNH_4^+$ clusters serve as internal calibrants. By examining the difference in mass between an ammonium cluster and a nearby *t*-butyl cluster, it is possible to determine whether chlorine is included in the cluster. Table 6.1 shows a partial list of exact masses of *tert*-butyl water clusters determined by using the ammonium water clusters as internal standards.

Table 6.1. Experimentally determined masses of *tert*-butyl containing water clusters.

Number of Waters for Cluster Containing:		
$C_4H_9^+$	C_4H_9Cl	Experimental Mass
37	35	723.4502
38	36	741.4746
39	37	759.4785
40	38	777.5034
41	39	795.5013
42	40	813.5050
43	41	831.5249
44	42	849.5333
45	43	867.5376
46	44	885.5690
47	45	903.5625
48	46	921.5732
49	47	939.5734
50	48	957.5991
51	49	975.6141
52	50	993.6129
53	51	1011.6239
54	52	1029.6338
55	53	1047.6627
56	54	1065.6764
57	55	1083.6944
58	56	1101.6831
59	57	1119.7111
60	58	1137.6647
61	59	1155.6753
62	60	1173.6968

As an example, ten seconds after trapping, the $(H_2O)_{24}NH_4^+$ cluster has an exact mass of 450.288049 Da and is detected at 450.3324 m/z. The $(H_2O)_{21}(CH_3)_3COHH^+$ has an exact mass of 453.30297 Da, 3.014921 Da more than the ammonium water cluster, and the $(H_2O)_{20}(CH_3)_3CClH^+$ cluster would have an exact mass of 453.2585 Da, 2.970451 Da more than that of the ammonium water cluster. The observed cluster is at 453.345 m/z, 3.0126 mass units above the observed ammonium water cluster, and should therefore correspond to the *t*-butyl cation with 22 waters. This comparison was carried out on each grouping of clusters. For small *n*, the observed cluster masses correspond to protonated water clusters containing *t*-butyl hydroxide. However, for large *n*, the clusters correspond to protonated water clusters containing *t*-butyl chloride. This transition seems to occur around $n = 58$ to $n = 60$. The peak at 1137.965 m/z is the lightest peak to correspond more closely to $(H_2O)_n(CH_3)_3CClH^+$ than to $(H_2O)_{n-1}(CH_3)_3COHH^+$. This would then be an $n = 58$ cluster. The larger mass peaks observed also correspond to $(H_2O)_n(CH_3)_3CClH^+$.

In addition, the isotope pattern of chlorine can be used to verify whether chlorine is present in a cluster. There is no indication of a ^{37}Cl peak distinguishable from the background until mass 757.567 Da, corresponding to $(H_2O)_{39}(CH_3)_3COHH^+$, is observed. The potential ^{37}Cl peak is 40% smaller than would be expected if the peak were composed solely of $(H_2O)_{37}(CH_3)_3CClH^+$. Subsequent clusters are associated with ^{37}Cl peaks, which are, on average, 50% the expected intensity. As the size of a water cluster increases, the lifetime of a water cluster decreases, which results in increased noise and makes it difficult to draw accurate conclusions regarding the isotopic ratio.[16] However, the exact mass data and the isotopic information indicate that between $n = 39$ and $n = 60$, both $(H_2O)_n(CH_3)_3COHH^+$ and $(H_2O)_{n+2}$ $(CH_3)_3CClH^+$ clusters are present in the spectrum. Smaller clusters evaporate HCl and only $(H_2O)_n(CH_3)_3COHH^+$ clusters are observed.

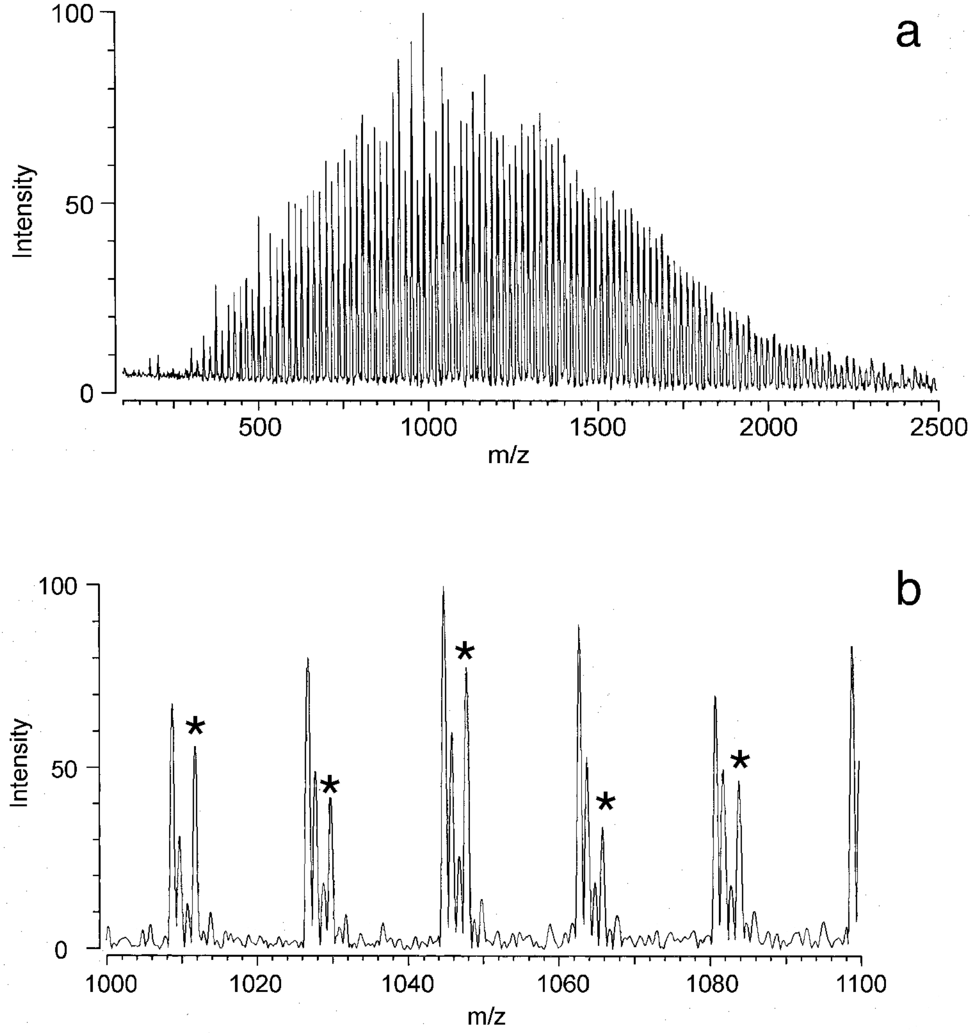

Figure 6.11. (a) Full cluster distribution 8 seconds after trapping. The major peaks in this spectrum are due to $(H_2O)_nNH_4H^+$. (b) Expansion of (a) to show peaks of interest. The starred peaks may correspond to $(H_2O)_nC_4H_9ClH^+$, $(H_2O)_{n+1}C_4H_9OHH^+$, or some combination of the two, where C_4H_9 refers to *t*-butyl.

The evaporation proceeds over time, but the naked *t*-butyl cation is not observed even after long periods of evaporation. Figure 6.12a shows the cluster distribution 78 seconds after trapping. The species $C_4H_9(H_2O)_2^+$ remains abundant after 798 seconds of trapping (the longest that the acquisition system allows), as shown in Figure 6.12b.

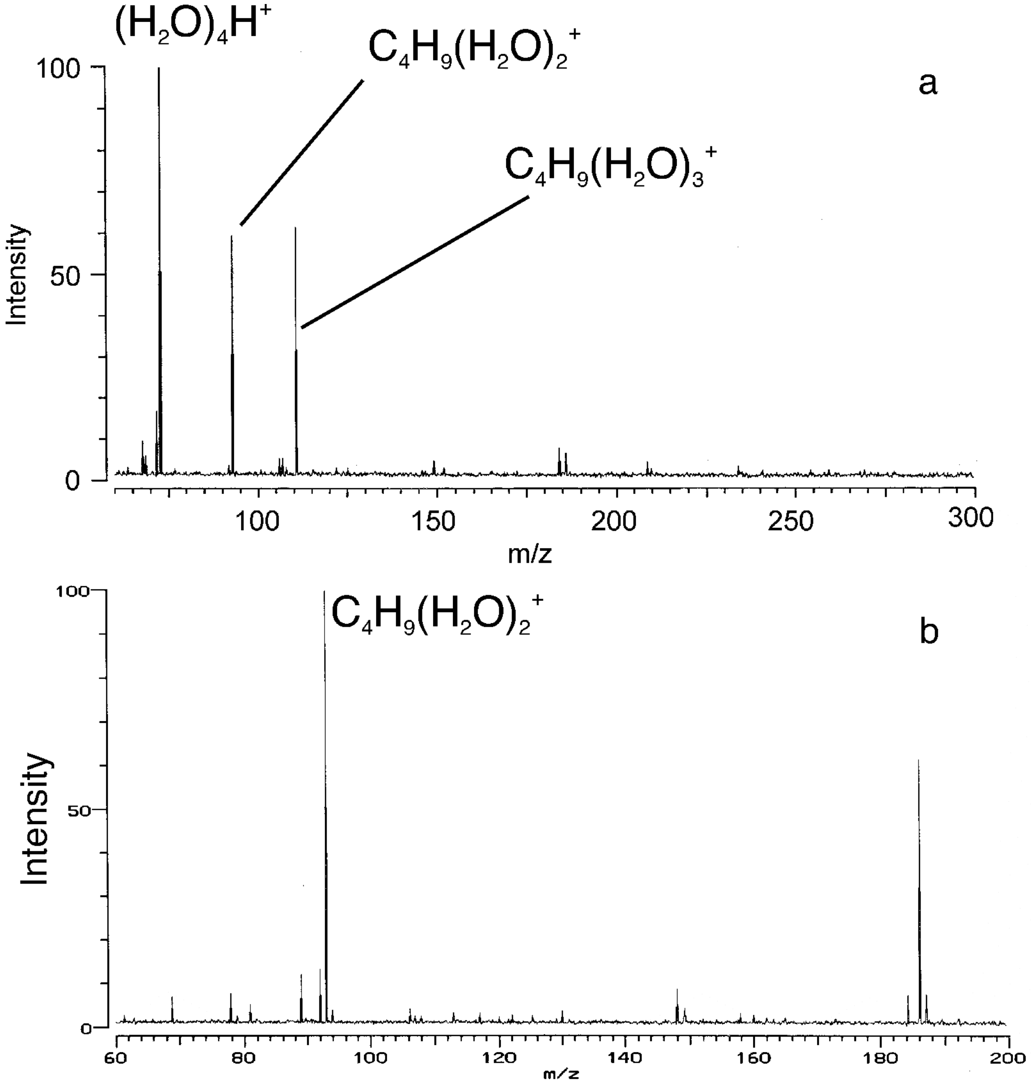

Figure 6.12. (a) Cluster distribution 78 seconds after trapping. The peak corresponding to $C_4H_9(H_2O)_2^+$ remains after all other peaks disappear, and is abundant even after 798 seconds of trapping, as shown in (b).

Hiraoka and Kebarle previously studied the enthalpy of hydration of the *t*-butyl cation.[39] They used the first enthalpy of hydration to determine that the product of the first hydration is protonated *t*-butanol, since the heat of formation of protonated *t*-butanol is identical to the heat of formation of the $C_4H_9H_2O^+$ species formed by hydration of the *t*-butyl cation. These measurements had to be made while the concentration of both species was decreasing at a constant rate, because there was no point at which the system reached a stable equilibrium. In addition, they were unable to measure the enthalpy of hydration of the protonated *t*-butanol, because there were no conditions under which the two species would equilibrate; the concentration of protonated *t*-butanol would always decrease and the $C_4H_9(H_2O)_2^+$ species would always increase in concentration. Measurements on higher hydrates showed that the higher hydrates are more stable toward dissociation of one water molecule than $C_4H_9(H_2O)^+$.

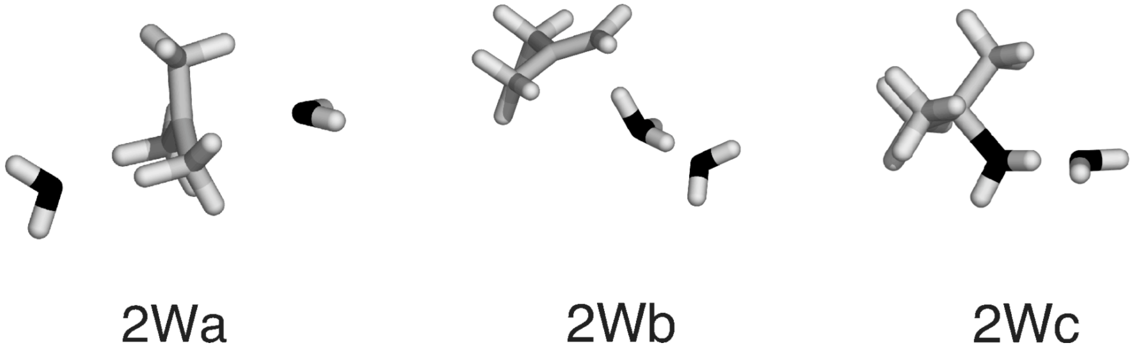

Figure 6.13. B3LYP 6-311++G optimized structures for $C_4H_9(H_2O)_2^+$. The lowest-energy structure is 2Wc, where protonated *t*-butanol is associated with a water molecule. Structure 2Wa has the waters solvating the *t*-butyl cation and is 38 kJ/mol less stable than 2Wc. The structure 2Wb would be an intermediate structure to isobutene, and is 69 kJ/mol less stable than 2Wc.**

Calculations on the $C_4H_9(H_2O)_2^+$ species indicate that the most stable structure is one in which a water molecule is closely associated with protonated *t*-butanol, shown as **2Wc** in Figure 6.13. In the monomeric water species, $C_4H_9(H_2O)^+$, the distance between the tertiary carbon and the oxygen of the water is 1.73 Å, while that distance decreases in the $C_4H_9(H_2O)_2^+$ species to 1.59 Å. The charge densities on the water monomer and water dimer of the *t*-butyl cation were examined by doing a PM5 calculation to determine charge densities. In the $C_4H_9(H_2O)^+$ system, the partial charge on the tertiary carbon is 0.254, while in the $C_4H_9(H_2O)_2^+$ system, the partial charge on the tertiary carbon is 0.191 (very similar to the charges calculated for the methyl hydrogens). The additional water molecule helps to stabilize the protonated *t*-butanol molecule. In addition, $C_4H_9(H_2O)_2^+$ is more stable than $C_4H_9(H_2O)^+$ + H_2O by 75 kJ/mol. The additional stabilization of protonated *t*-butanol gained from the complexed water molecule is enough that evaporation does not proceed from this highly stable structure.

In a large droplet system, *t*-butyl chloride is present, most probably in a "relay network" consisting of solvated *t*-butyl cation, a chloride anion, and a hydronium ion. Between $n = 39$ and $n = 60$, HCl is evaporated from the cluster, and smaller clusters have the empirical formula $C_4H_9(H_2O)_n^+$. These clusters are most likely composed of *t*-butanol, a hydronium ion, and water molecules. As the clusters evaporate, they gradually reach the most stable species, $C_4H_9(H_2O)_2^+$, corresponding to the structure labeled 2Wc in Figure 6.13.

6.4. Conclusions

Solvation patterns of ions can be used to discriminate between various constitutional isomers. Such patterns may even be useful in understanding how chiral information is disseminated through solutions. Solvation patterns of alkylammonium ions suggest that such quaternary ions, which are unable to participate in a hydrogen bond network, can be enclathrated in water clathrate structures if their size is compatible with such enclathration, or, alternatively, can form an ion-cluster complex with a water clathrate. Longer alkyl chains reduce the intensity of stable species in the solvated spectra, as the ion cannot effectively interact with water through a long alkyl chain. It also seems that dicationic species solvate positively charged sites in an alternating fashion, in agreement with previous studies on dianionic and dicationic species.

Finally, the solvolysis of *t*-butyl chloride has been observed in small water clusters, the first observation of this kind. The *t*-butyl chloride species is present only in relatively large droplets. Once the chlorine atom is displaced from the *t*-butyl species, reaction probably occurs quickly to yield *t*-butanol. HCl evaporates preferentially from the cluster once it is formed, since it has only one proton with which to hydrogen bond and binds more weakly than water ligands.[22] The species $C_4H_9OH(H_2O)H^+$ is exceptionally stable, as the additional water molecule helps stabilize the charge on a proton, and this species does not undergo further evaporation to yield protonated *t*-butanol.

6.5. References

(1) Czerwenka, C.; Maier, N. M.; Lindner, W. *Anal. Bioanal. Chem.* **2004**, *379*, 1039.

(2) Tao, W. A.; Zhang, D.; Wang, F.; Thomas, P. D.; Cooks, R. G. *Anal. Chem.* **1999**, *71*, 4427.

(3) Ramirez, J.; He, F.; Lebrilla, C. B. *J. Am. Chem. Soc.* **1998**, *120*, 7387.

(4) Grigorean, G.; Ramirez, J.; Ahn, S. H.; Lebrilla, C. B. *Anal. Chem.* **2000**, *72*, 4275.

(5) Fountain, S. T.; Lubman, D. M. *Anal. Chem.* **1993**, *65*, 1257.

(6) Testa, B.; Kier, L. B.; Cheng, C.-K. *J. Chem. Inf. Comput. Sci.* **2002**, *42*, 712.

(7) Fidler, J.; Rodger, P. M.; Rodger, A. *J. Am. Chem. Soc.* **1994**, *116*, 7266.

(8) Kier, L. B.; Cheng, C.-K.; Testa, B. *J. Chem. Inf. Comput. Sci.* **2003**, *43*, 255.

(9) Burkett, S. L.; Davis, M. E. *J. Phys. Chem.* **1994**, *98*, 4647.

(10) Franks, F., Ed. *Water: A Comprehensive Treatise*; Plenum: New York, 1975; Vol. 4.

(11) Kanno, H.; Ohnishi, A.; Tomikawa, K.; Yoshimura, Y. *J. Raman Spectrosc.* **1999**, *30*, 705.

(12) Blades, A. T.; Klassen, J. S.; Kebarle, P. *J. Am. Chem. Soc.* **1996**, *118*, 12437.

(13) Meot-Ner, M.; Deakyne, C. A. *J. Am. Chem. Soc.* **1985**, *107*, 469.

(14) Ding, C.-F.; Wang, X.-B.; Wang, L.-S. *J. Phys. Chem. A* **1998**, *102*, 8633.

(15) Yang, X.; Fu, Y.-J.; Wang, X.-B.; Slavícek, P.; Mucha, M.; Jungwirth, P.; Wang, L.-S. *J. Am. Chem. Soc.* **2004**, *126*, 876.

(16) Bondybey, V. E.; Beyer, M. K. *Int. Rev. Phys. Chem.* **2002**, *21*, 277.

(17) Gilligan, J. J.; Castleman, A. W., Jr. *J. Phys. Chem. A* **2001**, *105*, 5601.

(18) Buck, U.; Steinbach, C. *J. Phys. Chem. A* **1998**, *102*, 7333.

(19) Beyer, M.; Berg, C.; Gorlitzer, H. W.; Schindler, T.; Achatz, U.; Albert, G.; Niedner-Schatteburg, G.; Bondybey, V. E. *J. Am. Chem. Soc.* **1996**, *118*, 7386.

(20) Berg, C.; Beyer, M.; Achatz, U.; Joos, S.; Niedner-Schatteburg, G.; Bondybey, V. E. *Chem. Phys.* **1998**, *239*, 379.

(21) Beyer, M.; Achatz, U.; Berg, C.; Joos, S.; Niedner-Schatteburg, G.; Bondybey, V. E. *J. Phys. Chem. A* **1999**, *103*, 671.

(22) Fox, B. S.; Beyer, M. K.; Achatz, U.; Joos, S.; Niedner-Schatteburg, G.; Bondybey, V. E. *J. Phys. Chem. A* **2000**, *104*, 1147.

(23) Achatz, U.; Joos, S.; Berg, C.; Schindler, T.; Beyer, M. K.; Albert, G.; Niedner-Schatteburg, G.; Bondybey, V. E. *J. Am. Chem. Soc.* **1998**, *120*, 1876.

(24) Tanaka, K.; Mackay, G. I.; Payzant, J. D.; Bohme, D. K. *Can. J. Chem.* **1976**, *54*, 1643.

(25) Olmstead, W. N.; Brauman, J. I. *J. Am. Chem. Soc.* **1977**, *99*, 4219.

(26) Bohme, D. K.; Raskit, A. B. *J. Am. Chem. Soc.* **1984**, *106*, 3447.

(27) Ohta, K.; Morokuma, K. *J. Phys. Chem.* **1985**, *89*, 5845.

(28) Mohamed, A. A.; Jensen, F. *J. Phys. Chem. A* **2001**, *105*, 3259.

(29) Uggerud, E.; Bache-Andreassen, L. *Chem. Eur. J.* **1999**, *5*, 1917.

(30) Jorgensen, W. L.; Buckner, J. K.; Huston, S. E.; Rossky, P. J. *J. Am. Chem. Soc.* **1987**, *109*, 1891.

(31) Yamabe, S.; Tsuchida, N. *J. Comput. Chem.* **2004**, *25*, 598.

(32) Okuno, Y. *J. Phys. Chem. A* **1999**, *103*, 190.

(33) Rodgers, M. T.; Campbell, S.; Marzluff, E. M.; Beauchamp, J. L. *Int. J. Mass Spectrom. Ion Processes* **1994**, *137*, 121.

(34) Lee, S.-W.; Freivogel, P.; Schindler, T.; Beauchamp, J. L. *J. Am. Chem. Soc.* **1998**, *120*, 11758.

(35) Khan, A. *Chem. Phys. Lett.* **1994**, *217*, 443.

(36) Wei, S.; Shi, Z.; Castleman, A. W., Jr. *J. Chem. Phys.* **1991**, *94*, 3268.

(37) Lee, S.-W.; Cox, H. A.; Goddard, W. A., III; Beauchamp, J. L. *J. Am. Chem. Soc.* **2000**, *122*, 9201.

(38) Kuba, A.; Hawlicka, E. *Phys. Chem. Chem. Phys.* **2003**, *5*, 4858.

(39) Hiraoka, K.; Kebarle, P. *J. Am. Chem. Soc.* **1977**, *99*, 360.